Solvent-induced Inversion of Colloidal Aggregation During Electrophoretic Deposition

Justin R. DeMoulpied,[1] Jessica A. Killenbeck,[1] Zebulon G. Schichtl,[1] Babloo Sharma,[1] Susanne Striegler,[1] and Robert H. Coridan[1,2*]

[1] Department of Chemistry and Biochemistry, University of Arkansas, Fayetteville AR 72701

[2] Materials Science and Engineering Program, University of Arkansas, Fayetteville AR 72701

* rcoridan@uark.edu

Abstract: Electrophoretic deposition of colloidal particles is a practical system for the study of crystallization and related physical phenomena. The aggregation is driven by the electroosmotic flow fields generated by the polarization of the electrode-particle-electrolyte interface. Here, we report on the electrochemical control of aggregation and repulsion in the electrophoretic deposition of colloidal microspheres. The nature of this transition depends solely on the composition of the solvent. The observed behavior switches between electrical field-driven aggregation in water to electrical field-driven repulsion in ethanol for otherwise identical systems of colloidal microspheres. This work uses optical microscopy-derived particle and a recently developed particle insertion method-approach to extract the effective interparticle potentials as a function of the solvent and electrode potential at the electrode interface. This approach can be used to understand the phase behavior of these systems based on the observable particle positions rather than a detailed understanding of the electrode-electrolyte microphysics.

Electrophoretic deposition (EPD) is a common method for controlling the composition of functional surface coatings on electrodes.[1,2] A model system for studying EPD is the directed assembly of particle layers from solutions of chemically synthesized, monodisperse microspheres.[3,4] Research in this area has focused primarily on the mechanism for observed aggregation and the related phase behavior.[5–7] Aggregation is counterintuitive when considering the electrostatic repulsion between like-charged particles requisite for the stability of the colloidal suspension.[8] The driving force for the observed aggregation during EPD is the complex interaction between the electrode, the electrolyte, and the particle surface rather than a true interparticle attraction.[9,10] Electrical polarization induces electroosmotic flow normal to the electrode-fluid interface without particles on the surface. This flow becomes inhomogeneous around microspheres on the electrode surface, generating a component of flow parallel to the electrode surface.[9,11] The resulting flow entrains nearby particles, generating sufficient force to drive them into close-approach aggregation.[12,13] These interactions can be modulated via both DC and AC electric fields to form dense layers of disordered and crystalline phases in aqueous colloidal suspensions.[14–17] The electric field-induced aggregation of colloidal particles drives behaviors characteristic of a variety of dynamical physical phenomena, including nucleation, phase transitions, annealing, and crystal growth.[18] EPD is therefore a useful approach for studying these phenomena. Here, we report on an electrolyte-driven inversion of the in-plane interparticle forces during electrophoretic deposition. In water, SiO_2 microspheres on electrodes show the electric field driven aggregation and crystallization dynamics that are well documented for the system.[3,19] Replacing the aqueous solvent with ethanol resulted in an effective

repulsion between particles while maintaining an attraction to the electrode surface. The behavior is analogous to a Wigner glass phase observed in soft matter systems where particles exhibit long-range, electrostatic repulsion, yet are confined to a neutralizing background.[20–24] The observed repulsion in ethanol was reversible under the control of the applied potential difference. To characterize these phases under EPD, we used a recently developed particle insertion method approach to calculate an effective interparticle pair potential based on optical microscopy imaging experiments.[25] Ascribing a pair potential description to the interparticle interactions can produce quantifiable comparisons of relevant electrochemical effects on the observed phase behavior. The collective behavior of the dynamics and structure of the colloid-electrode interface can then be controlled deterministically without a direct representation of the complicated microphysics of the electroosmotic flow at the surface.

Figure 1a,b shows the aggregation of 7.75 μm silica microspheres (Cospheric) on a transparent, fluorine-doped tin oxide (FTO) electrode in an EPD microscopy cell filled with pure water. Initially, the microspheres were disorganized on the electrode surface due to sedimentation and the passive interparticle interactions. The spheres quickly aggregate under the influence of a 5.0 V cm^{-1} DC applied field between transparent electrodes (4 mm separation, Figure S1), with some regions forming two-dimensional hexagonally close-packed (HCP) crystalline domains (Figure 1b). The observed phase behavior was inverted when the solvent was changed from water to ethanol in an otherwise identically prepared system. High concentration ethanol solutions are often used in place of water during EPD to avoid the disruptive effects of electrolytic bubble evolution at high potentials. When a 7.5 V cm^{-1} field was applied in ethanol, we

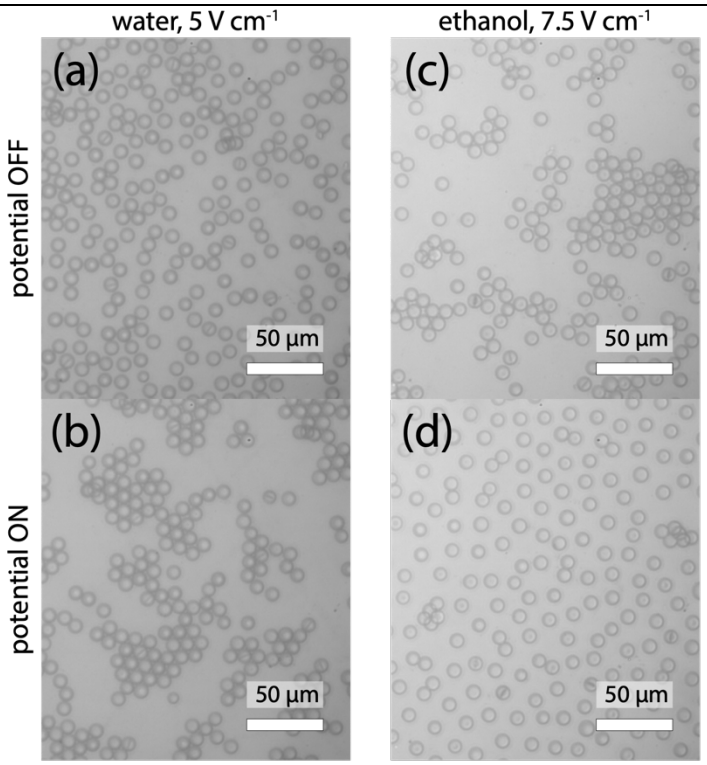

Figure 1 – (**a**,**b**) A dilute arrangement of 7.75 µm-diameter silica microspheres on the surface of an FTO electrode (a) before and (b) after applying a 5.0 V cm^{-1} electric field in water. The electric field drives aggregation between the particles. (**c**,**d**) An otherwise identical arrangement of 7.75 µm-diameter silica microspheres on the surface of an FTO electrode (c) before and (d) after applying a 7.5 V cm^{-1} electric field in ethanol. The electric field drives repulsion between the particles, but the attraction of the particles to the electrode surface is maintained.

observed a rapid transition to interparticle repulsion while maintaining an attraction to the electrode itself (Figure 1d). In both solvents, reversing the polarity of the applied electric field ejected the particles from the electrode surface. Movies of these examples are included in the supplemental information (Movie S2, Movie S4).

Quantitative differences in the organization of the microspheres were observed in the time-dependent pair distribution histogram, h(r,t), during optical microscopy

experiments. Experimental details and a description of the computational methodology are included in the Supplemental Information. The histogram h(r,t) was computed for each second of the experiment by binning the interparticle distances from centroid positions measured in each of the 50 frames imaged during that one second interval. The microsphere dynamics were sufficiently slow so that the one-second interval is considered to average out the noise from the particle tracking (Figure S2, for example). Given the slow motion of the particles, they can be treated as being in a steady state relatively quickly after the field is applied. A full profile of h(r,t) for an experiment where a 2.5 V cm^{-1} field is applied in an aqueous system is shown in Figure S3a. The initially disordered assembly in the field 'off' state (150 s, Fig 2a) increases in order after the field is applied (the 'on' state, 450 s, Fig 2a), as shown by the increase in the amplitude of the first coordination peak at 9 μm and in the appearance of a more pronounced second-order coordination peak at 16 μm. The assembly became more disordered when the field was turned off (900 s, Fig 2a), and only slightly reformed when the field was turned on again (1100 s, Fig 2a).

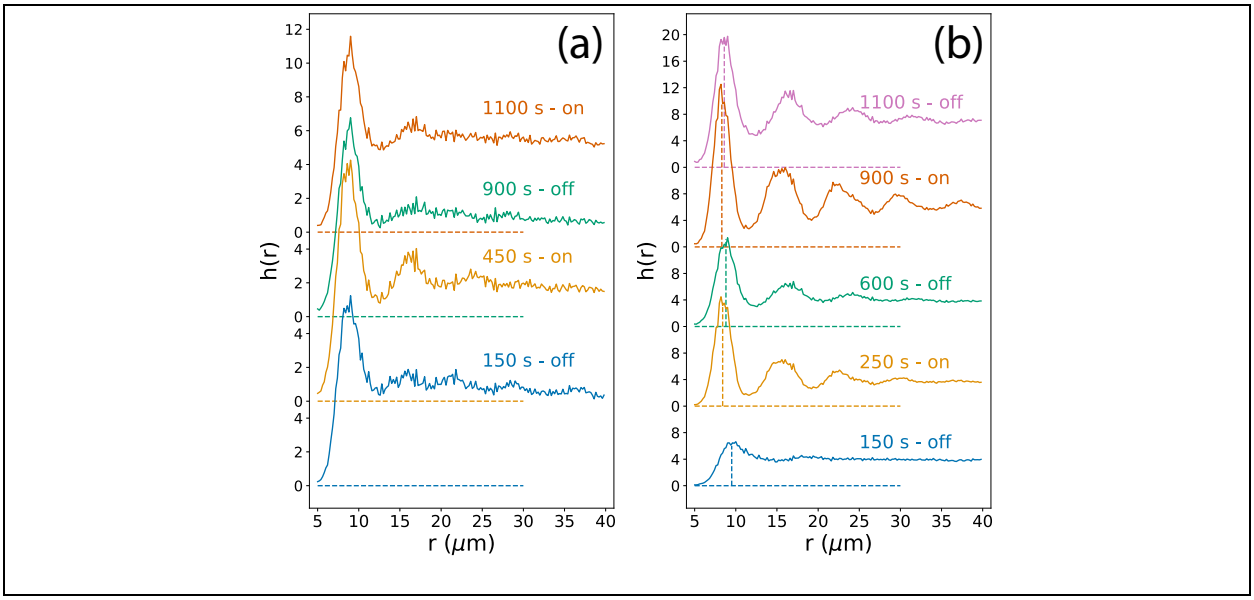

Figure 2 – Pair distribution histograms, h(r), of microspheres on an FTO electrode in water under the influence of (**a**) a 2.5 V cm^{-1} applied field and (**b**) a 5.0 V cm^{-1} applied field. 'On' and 'off' note whether the field was being applied at that point in the experiment.

A stronger effect was observed in the aqueous system when the applied field was increased to 5.0 V cm^{-1}. The full h(r,t) profile for the experiment in Figure 1 is shown in Figure S3b. Before the field was turned on, the spheres organized into the same relatively disordered structure driven by sedimentation onto the electrode (Figure 2b, 150 s). After turning on the field, the particles rapidly aggregated, as observed in Figure 1b and Figure 2b (250 s), with h(r) exhibiting a shift of the first coordination peak to lower *r* (8.4 μm, nearly the distance of closest approach for two microspheres) and a significant increase in the density. Multiple orders of coordination were also observed in h(r), consistent with the observed HCP arrangement of the spheres in the sparse two-dimensional layer.

Turning the field off (Figure 2b, 600 s) caused a melting of the crystalline structure, observed through the decline of the coordination peaks and a shift of the first coordination peak to longer interparticle distances (9.5 μm). The asymptotic h(r) continuously increased throughout the experiment as more microspheres joined the electrode surface through sedimentation and EPD. This behavior was reversible under repeated application (Figure 2b, 900 s) and release (Figure 2b, 1100 s) of the field. Experiments in water with a higher applied field (7.5 V cm^{-1}) resulted in the irreversible immobilization of microspheres on the electrode surface. The reversible crystallization of aqueous suspensions of microspheres on the electrode surface is consistent with

other experimental studies where strong aggregation was observed.[16] In the case of a highly charged colloid surface, like for silica in water (ζ = -40.8 mV), the flow is directed at the surface of the microsphere.[7] The flow entrains nearby particles, inducing the observed effective attraction.[12]

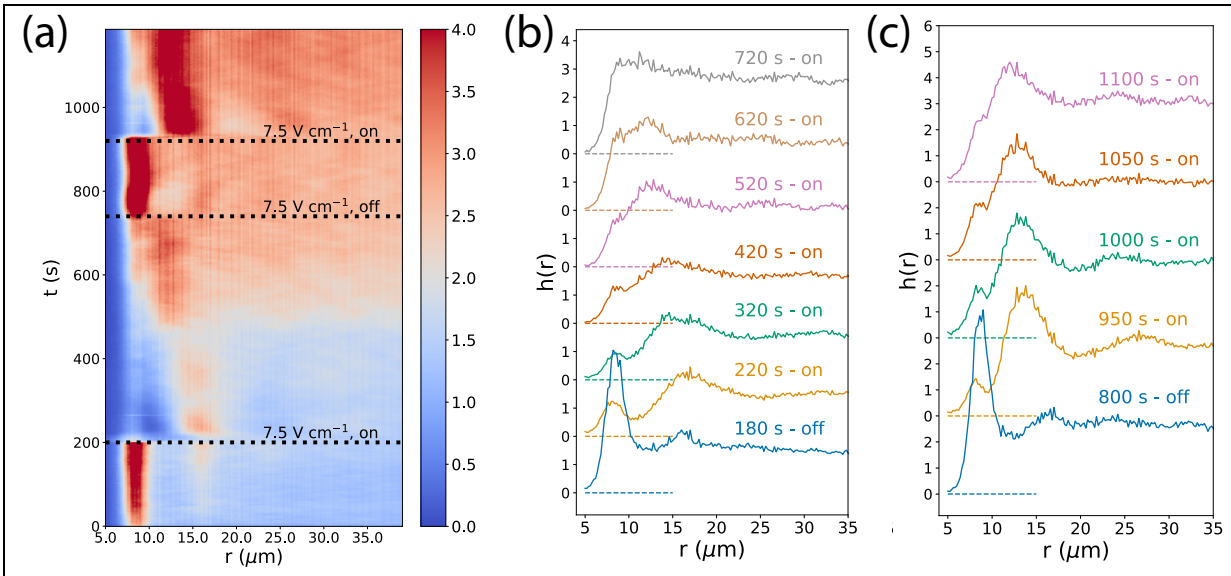

Figure 3 – (a) h(r,t) for silica microspheres in pure ethanol switching between the 'on' and 'off' state of a 7.5 V cm^{-1} applied electric field. (b) The time evolution of h(r) after switching the field on at 200 s. The Wigner glass-like phase appears as the shift of the maximum in the histogram to larger distances than close packing. The peak shifted to shorter interparticle distances as EPD progressed and the density of microspheres on the electrode surface increased. (c) The repulsion was reversible, as h(r) showed a close packing peak soon after the field was turned off at 750s. When it was turned on again at 925 s, the Wigner glass-like phase reappeared.

In ethanol, we observed an interparticle repulsion under the influence of the applied field of 7.5 V cm^{-1}. The pair distribution histogram h(r,t) for the experiment from Figure 1c,d is shown in Figure 3a. Microspheres were initially more ordered by sedimentation than

we had observed in water. The initial h(r) (Figure 3b, 180 s) showed a strong first coordination peak at r = 8.5 μm and a discernable second order coordination peak. After applying the electric field at 200 s, the microspheres immediately separate, migrating to maximize the distance between particles. A movie of this motion is shown in Movie S4. Microspheres were observed to avoid other spheres at distances longer than simple, hard sphere steric avoidance. h(r) is shown for selected points during the experiment in Figures 3b and 3c. A small fraction of pairs of spheres stayed in direct surface-to-surface contact after the potential was turned on, as indicated by the small peak at 8.5 μm. However, a significant majority of the microspheres exhibited this interparticle repulsion, and many of these pairs eventually separated. The structure of the repulsive phase is analogous to the formation of a two-dimensional Wigner glass, where the particles have a strong attraction to the surface and a Coulombic-like interparticle repulsion.[20] The physical nature of the repulsion observed in the microsphere-ethanol system is related to the predicted reversal of electroosmotic flow, directed away from the particle surface, for particles with no surface zeta potential.[6,12,26] There is no explicit electrolyte added to the ethanol, and the microspheres have a small zeta potential corresponding to an unstable colloidal suspension (ζ = -7.81 mV). The density of the Wigner glass-like phase increased as particles joined the electrode surface via EPD. While density increased over the period from 220 s to 720 s, the close-packed coordination shell in h(r) vanished. The first coordination shell of the Wigner glass-like phase gained density and broadened over time. The peak position shifted to smaller interparticle distances (16 μm at 220 s to 12 μm at 520 s) as the density of microspheres on the surface increased. When the potential was turned off at 760 s, the

slight attraction between microspheres returned, with corresponding increase in density from the extended period of EPD (Figure 3c, 800 s). Restoring the applied field at 920 s reformed the Wigner glass-like phase, with very little intensity observed for close-packed spheres (Figure 3c, 950 s -1100 s). A similar Wigner glass-like phase was observed for an electrode covered with a nearly conformal monolayer of close-packed microspheres in ethanol (Movie S5), though the effect was diminished due to the density of spheres on the electrode surface.

The nature of the transition between interparticle attraction in water and repulsion in ethanol on an electrode surface depends on the complex effects that the surface chemistry, solvent, and electrode potential have on the electroosmotic flow. An effective description of the interparticle interactions is practically useful for reducing this complex physical chemistry to the scale of the physically observable evolution of the system. It was recently demonstrated that model-free, effective interparticle pair potential functions can be derived from experimentally derived particle trajectories.[25] A Widom particle insertion method was used to calculate the i^{th}-iteration of the pair potential $g^{(i)}(r)$ from calculations based on the excess chemical potential, μ_{ex}, based on the guess of the effective pair potential $u_{eff}^{(i)}(r)$.[27–30] The pair potential is iteratively improved until the computed $g^{(i)}(r)$ converges to the experimental one. Details of the implementation of this approach are provided in the Supplemental Information. The model-free approach generates a pair potential function that describes the observed system and can be used to quantitatively understand the effects of the chemical and electrochemical environment in an intuitive way based on macroscopic, observable behavior.

We used this particle insertion approach to calculate the effective interparticle pair potential function, $u_{eff}(r)$, for microspheres in water, ethanol, and ethanol-water mixtures. The converged g(r) and corresponding $u_{eff}(r)$ are shown in Figure 4 as a function of the electrochemical environment. We computed the density-normalized pair distribution function g(r) (Figure 4a) from the iteratively determined $u_{eff}(r)$ (Figure 4b) for the field 'on' and field 'off' states for the water experiments described in Figure 2. The units of $u_{eff}(r)$ are arbitrary ($k_BT = 1$ for in the reconstructions), but the arbitrary units are consistent for each reconstruction. Some motion was observed when the electric field was turned on in the microscopy movie (Movie S1) and in the h(r,t) calculation (Figure S3a). Quantitatively, we observed only a small difference between the 'on' and 'off' states in g(r) or $u_{eff}(r)$ for the smaller applied field (2.5 V cm^{-1}). The potential minimum of the 'on' state was at a slightly lower interparticle distance (r_{min} = 9.4 μm) than for the 'off' state (r_{min} = 9.7 μm) at this bias. Differences in the depths of the potential minima ($u_{eff}(r_{min})$ = -1.2) and the range of the attractive well (r < 30 μm) were negligible between the 'on' and 'off' state.

For higher applied field in water (5.0 V cm^{-1}), the difference in $u_{eff}(r)$ between the 'on' and 'off' states was much more significant. $u_{eff}(r)$ for the 'off' state should be identical to u(r) for the 'off' state for the 2.5 V cm^{-1} experiment, but the depth of the potential at r_{min} was only $u(r_{min})$ = -0.85. We attribute this to a slightly lower observed particle density in this experiment. Additionally, it is not particularly apt to describe this inactive state of the system by an interparticle potential. However, the extracted potentials were quantitatively similar in r_{min} = 9.6 μm and range of attraction (r < 30 μm). For the field 'on' state, r_{min} shifted significantly to a lower interparticle distance (8.8 μm) and a deeper

potential minimum, $u_{eff}(r_{min})$ = -2.2. This quantitative difference can be used to compare the electrochemical and environmental effects interactions between particles. The reconstruction of $u_{eff}(r)$ for this 'on' state is noisier and has additional local minima at larger interparticle separations, even though we used a significantly larger number of particle insertions (10^5 insertions for the 'on' state here versus $6x10^3$ for the 'off' state) for each $u_{eff}(r)$ iteration. Particle insertion methods are known to have inaccuracies when studying dense systems due to the outsized sampling of low-probability configurations with overlapping particles.[31–34]

We observed significant differences in $u_{eff}(r)$ for the experiments that used ethanol for solvent rather than water. The silica microparticles were more aggregated in ethanol prior to the application of electric field (in the 'off' state) than in water. The reduced zeta potential of silica in ethanol can explain this observed increase in passive aggregation. The difference resulted in a $u_{eff}(r)$ with a smaller minimum distance, r_{min} = 8.8 μm, a slightly deeper minimum, $u_{eff}(r_{min})$ = -1.4, and a shorter range of attraction ($r < 17$ μm) than observed in water. This is a pair potential description of the passive 'off' state at t = 180 s (Figure 4d). The 7.5 V cm^{-1} applied field was turned on at 200 s and the Wigner glass-like phase formed within 10 s. The $u_{eff}(r)$ for this initial 'on' state (220 s in Figure 4d) was shallower ($u_{eff}(r_{min})$ = -0.8), with r_{min} shifted out to 20.5 μm for this part of the experiment. A small local minimum in $u_{eff}(r)$ was observed at the close-contact distance, but this was in the absolute repulsive portion of the pair potential. As EPD gradually increased the density of microspheres on the surface, the potential minimum shifted to correspondingly lower distances (r_{min} = 14 μm for the experiment at 520 s, still in the 'on' state). However, close contact between microspheres remained in the

repulsive portion of the potential. Reconstructions for $u_{eff}(r)$ periods when the electric field was turned off (800 s, Figure 4d), and reinstated (950 s, Figure 4d) show that the Wigner glass-like phase is reversible under switching electric fields.

We observed the transition from the glass-like phase to colloidal crystallization for microsphere under applied fields of 7.5 V cm^{-1} in ethanol-water solutions. The zeta potential of the silica particles increased with the addition of water (ζ = -20.6 mV for 95% ethanol/5% water, ζ = -37.6 mV for 50% ethanol/50% water), indicating an increasing surface charge on the microspheres. The transition was observed in microscopy imaging. Motion indicating a slight repulsion was observed in the 95% ethanol solution (Movie S6) and particle aggregation was observed in the 50% ethanol solution (Movie S7). The g(r) and $u_{eff}(r)$ for each experiment are shown in Figures 4e and 4f, respectively. For the 95% ethanol solution, $u_{eff}(r)$ resembled a linear combination of the potentials for a close-packed phase (r_{min} = 9.4 μm) and the Wigner glass-like phase (r_{min} = 14 μm). In a 50% ethanol solution, $u_{eff}(r)$ resembled the observed behavior in pure water, with a deep minimum (r_{min} = 8.1 μm, $u_{eff}(r_{min})$=-2.6). The particles remained mobile on the electrode surface, where they had become pinned in pure water under the same applied field. The dense clusters of microspheres in the 50% ethanol solution resulted in a noisy profile and artificial local minima in $u_{eff}(r)$ like the one observed in the pure water.

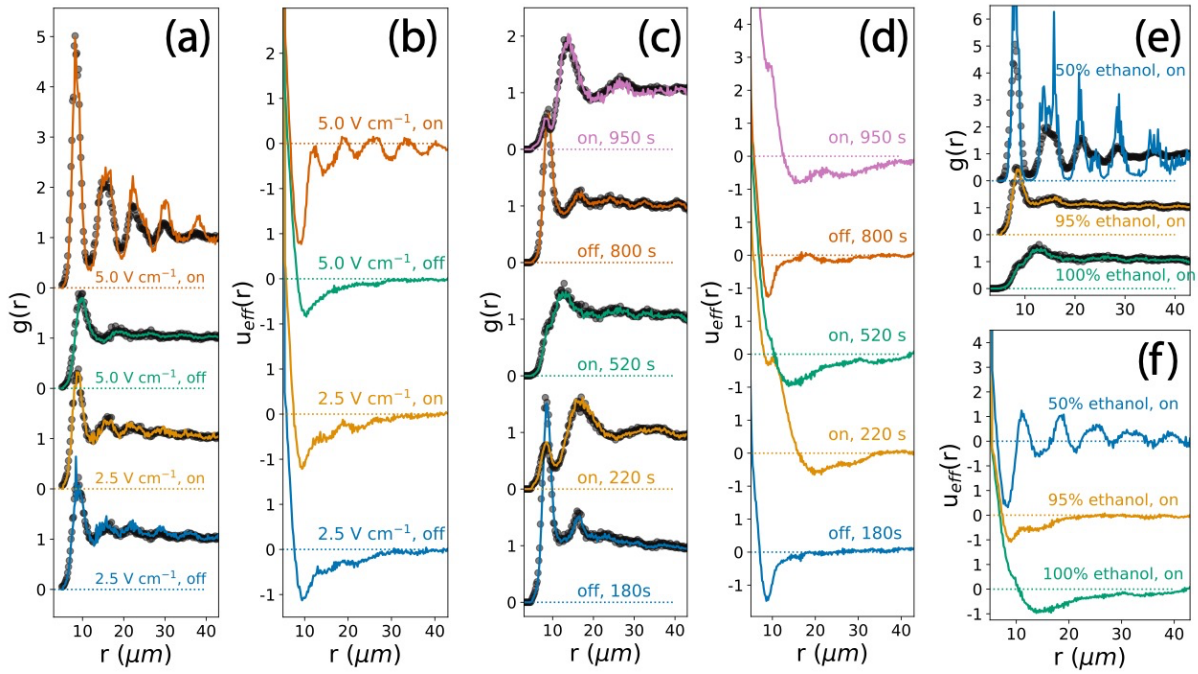

Figure 4 – (a) g(r) and (b) $u_{eff}(r)$ for silica microspheres in pure water (Figure 2). (c) g(r) and (d) $u_{eff}(r)$ for silica microspheres in ethanol (Figure 3) under the influence of an applied field of 7.5 V cm^{-1}. (e) g(r) and (f) $u_{eff}(r)$ for silica microspheres in ethanol-water mixtures under the influence of an applied 7.5 V cm^{-1} field. The 100% ethanol potential is the same as the 520 s example from (d). Each $u_{eff}(r)$ and corresponding g(r) were computed from between six and eight iterations of the particle insertion methods described in the Supporting Information. g(r) was computed iteratively from N = 6000 particle insertions in every case except for the '5.0 V cm^{-1}, on' and '50% ethanol, on' cases (N = 100000) due to the noted convergence issues with dense systems. Convergence was determined by the iteration with the minimum root-mean-squared error between experimental g(r) (black circles) and the insertion method-calculated g(r) (solid lines).

These results demonstrate that the particle insertion method can be used to discern the effective interactions between particles in these dilute systems. To our knowledge, this is the first explicit measurement of the empirical interparticle potential between colloids during aqueous EPD. We have also used this approach to discern the effective or the long-ranged repulsion between colloids in the Wigner crystal-like phase. effective potentials, $u_{eff}(r)$ showed reversible sensitivity to changes in the electrochemical environment, including the electrode potential and solvent composition. These effects are borne out in physically intuitive and quantifiable ways, such as in the depth of the attractive potential well for aggregating systems, and the ranges of the attraction, and the softness of the repulsive Wigner glass-like phase. This approach could also be made more accurate in dense systems of microspheres through the implementation of methods that take this into account.[35,36]

The extraction of a pair potential from an empirically determined pair distribution may seem like a matter of self-consistency. The particle insertion method generates a function, $u_{eff}(r)$, that satisfies and is completely dependent on the measured g(r). Empirical pair potentials like the ones derived in this work are critical for computational studies of the phase behavior and directed assembly of colloidal systems. While the microspheres in this system were relatively simple, monodisperse particles, they showed very different phase behaviors under similar electrochemical control based on the solvent composition. The experimental measurement of $u_{eff}(r)$ from microscopy data captures the subtle differences in interactions that can be used directly in computational studies. The microphysics driving the motion of the system is embedded in these functions. More complex interactions, such as non-spherical particles, patchy particles,

or multicomponent systems can be addressed in similar mixed experimental-theoretical approaches.[37,38]

In summary, we have shown that the underlying electrode-fluid interactions generate a repulsive, Wigner glass-like phase behavior for microspheres in ethanol. This is an inversion of the electrode-driven aggregation behavior observed in an otherwise identical microsphere-electrode system in water. Extracting the pair distribution function of the microspheres as a function of time enables us to calculate the effective pair potential guiding the system evolution, which allows for straightforward and intuitive comparisons between the phase behavior and the chemical environment without explicit knowledge of the underlying microscopic physics driving the particles' motions. This approach to modeling the behavior with interparticle potentials also facilitates simple coarse-grained simulations of these systems to improve our understanding of electrophoretic deposition for the development of functional colloidal interfaces.

Experimental Section

Materials and Methods

Water (HPLC grade; BDH) and ethanol (200 proof; EMD Millipore) were used as received. Silica microspheres (7.75 μm) and nanospheres (166 nm) were purchased as a dry powder (Cospheric) then suspended in the solvent by sonication. The nominal concentration of the microspheres was chosen to limit the surface coverage of spheres on the electrode surface to less than one monolayer. In storage, we observed that the microspheres sedimented from the solution in the vials. Prior to any imaging experiments each solution was sonicated in order to resuspend the microspheres to the desired concentration.

Optical microscopy measurements were performed with an Olympus BX 53 microscope equipped with a long working distance 50x objective lens, a multiwavelength LED illuminator (PE-4000, CoolLED), and a high-speed camera (IL-5, Fastec). Zeta potential measurements were performed with a Zetasizer Nano ZS (Malvern Panalytical) equipped with a 632.8 nm He-Ne laser, an autosampler, and the Malvern Zetasizer Software, version 7.13 for data collection and analysis.

Zeta potential measurements

Zeta potential measurements were obtained at 25 °C using clear disposable folded capillary cells filled with sample and solvent, respectively. The zeta potentials were measured using the Smoluchoeski model implemented in the software with a F(κa) value of 1.50. The data were recorded for settings of the material as silica nanoparticles (166 nm) with a refractive index (RI) of 1.46 and an absorbance of 0.0. Silica nanoparticles were used to avoid sedimentation during the zeta potential measurement

but are assumed to be sufficiently representative of the zeta potential of the surfaces of microspheres prepared in the same way and provided by the same manufacturer. Each solution of nanoparticles was prepared for the zeta potential measurement at a particle concentration of 1.0 mg mL^{-1}. The refractive index, viscosity (cP), and dielectric constant (ε), of the respective dispersant were selected for each solvent for zeta potential data analysis are shown in Table S1. Each sample was equilibrated for 120 s and measured five times as an average of 10 to 100 accumulations each without delay between measurements. The reported zeta potential data are given as an average of five measurements (Table S2).

Collection of optical microscopy data and analysis

Optical microscopy imaging experiments were performed in a cell built from glass slide electrodes coated with a conductive layer of fluorine-doped tin oxide (FTO, MTI Corp.). A 4 mm HDPE spacer with a 1 cm hole for the imaging volume was epoxied (Hysol 9460) to one of the slides and cured overnight at 50 ºC before use. Between experiments, the FTO electrodes were sonicated in pure ethanol to remove any residual microspheres then dried under compressed air. The solutions of silica microspheres were sonicated prior to being added to the cell, then sealed with another FTO electrode on top. The imaging volume was slightly overfilled with the solution to assure uniform electrolyte contact and conductivity between the electrodes. The electrodes were sealed by pressure clips and held flat with respect to imaging geometry (Figure S1). The potential between the electrodes was controlled by a standard DC power supply (Tekpower TP1803D). Imaging experiments were performed with monochromatic (550

nm) illumination as the light source for reflection imaging. The camera was set to generate 2560 x 2048 tiff images at 50 frames per second (fps) with 12-bit depth. Python scripts using the OpenCV library were developed to identify individual particles in the field of view. The 50 fps frame rate was significantly faster than the dynamics of particle motion, so any errors in identifying the centroid of each particle in the frame was averaged out in the multiframe averaging use in the analysis. As described in the main text, the pair distribution histogram h(r,t) was calculated from the pairwise distances between particles in each frame with a bin size of 0.2 μm. h(r,t) was computed by binning 50 consecutive frames into the analysis for each second of the experiment. During some experiments, the cell shifted slightly causing the field of view to change, though this is averaged out of the pair distribution function analysis as well.

Supporting Information

Descriptions of the experimental and theoretical methods, including schematics of the microscopy cell and examples of microscopy data/movies.

Acknowledgements

RHC acknowledges support from the National Science Foundation under Grant No. 1934725. SS acknowledges support from the NSF under Grant No. CHE-1854304 for procurement of the DLS instrumentation used in this work.

[1] A. R. Boccaccini, J. H. Dickerson, *J. Phys. Chem. B* **2013**, *117*, 1501.
[2] P. Amrollahi, J. S. Krasinski, R. Vaidyanathan, L. Tayebi, D. Vashaee, in *Handb. Nanoelectrochemistry Electrochem. Synth. Methods Prop. Charact. Tech.* (Eds: M. Aliofkhazraei, A.S.H. Makhlouf), Springer International Publishing, Cham, **2016**, pp. 561–591.
[3] M. Holgado, F. García-Santamaría, A. Blanco, M. Ibisate, A. Cintas, H. Míguez, C. J. Serna, C. Molpeceres, J. Requena, A. Mifsud, F. Meseguer, C. López, *Langmuir* **1999**, *15*, 4701.
[4] A. L. Rogach, N. A. Kotov, D. S. Koktysh, J. W. Ostrander, G. A. Ragoisha, *Chem. Mater.* **2000**, *12*, 2721.
[5] Böhmer, *Langmuir* **1996**, *12*, 5747.
[6] Y. Solomentsev, M. Böhmer, J. L. Anderson, *Langmuir* **1997**, *13*, 6058.
[7] Y. Solomentsev, M. Bevan, J. L. Anderson, *Langmuir* **2000**, *16*, 9208.
[8] D. F. Evans, H. Wennerström, *The Colloidal Domain: Where Physics, Chemistry, Biology, and Technology Meet*, Wiley-VCH, New York, **1999**.
[9] P. J. Sides, *Langmuir* **2003**, *19*, 2745.
[10] L. Besra, M. Liu, *Prog. Mater. Sci.* **2007**, *52*, 1.
[11] S. M. H. Hashemi Amrei, S. C. Bukosky, S. P. Rader, W. D. Ristenpart, G. H. Miller, *Phys. Rev. Lett.* **2018**, *121*, 185504.
[12] D. C. Prieve, P. J. Sides, C. L. Wirth, *Curr. Opin. Colloid Interface Sci.* **2010**, *15*, 160.
[13] C. L. Wirth, R. M. Rock, P. J. Sides, D. C. Prieve, *Langmuir* **2011**, *27*, 9781.
[14] P. J. Sides, *Langmuir* **2001**, *17*, 5791.
[15] M.-G. Song, K. J. M. Bishop, A. O. Pinchuk, B. Kowalczyk, B. A. Grzybowski, *J. Phys. Chem. C* **2010**, *114*, 8800.
[16] C. S. Dutcher, T. J. Woehl, N. H. Talken, W. D. Ristenpart, *Phys. Rev. Lett.* **2013**, *111*, 128302.
[17] S. Saini, S. C. Bukosky, W. D. Ristenpart, *Langmuir* **2016**, *32*, 4210.
[18] P. Sarkar, D. De, K. Yamashita, P. S. Nicholson, T. Umegaki, *J. Am. Ceram. Soc.* **2000**, *83*, 1399.
[19] R. C. Hayward, D. A. Saville, I. A. Aksay, *Nature* **2000**, *404*, 56.
[20] D. Bonn, H. Tanaka, G. Wegdam, H. Kellay, J. Meunier, *EPL Europhys. Lett.* **1999**, *45*, 52.
[21] B. Ruzicka, L. Zulian, E. Zaccarelli, R. Angelini, M. Sztucki, A. Moussaïd, G. Ruocco, *Phys. Rev. Lett.* **2010**, *104*, 085701.
[22] R. Angelini, E. Zaccarelli, F. A. de Melo Marques, M. Sztucki, A. Fluerasu, G. Ruocco, B. Ruzicka, *Nat. Commun.* **2014**, *5*, 4049.
[23] T. B. Becher, C. B. Braga, D. L. Bertuzzi, M. D. Ramos, A. Hassan, F. N. Crespilho, C. Ornelas, *Soft Matter* **2019**, *15*, 1278.
[24] G. Porpora, F. Rusciano, V. Guida, F. Greco, R. Pastore, *J. Phys. Condens. Matter* **2020**, *33*, 104001.
[25] A. E. Stones, R. P. A. Dullens, D. G. A. L. Aarts, *Phys. Rev. Lett.* **2019**, *123*, 098002.
[26] W. D. Ristenpart, I. A. Aksay, D. A. Saville, *Langmuir* **2007**, *23*, 4071.
[27] B. Widom, *J. Stat. Phys.* **1978**, *19*, 563.
[28] D. Frenkel, B. Smit, *Understanding Molecular Simulation*, Elsevier, **2002**.

[29] R. P. A. Dullens *, D. G. A. L. Aarts, W. K. Kegel, H. N. W. Lekkerkerker, *Mol. Phys.* **2005**, *103*, 3195.
[30] N. Chennamsetty *, H. Bock, K. E. Gubbins, *Mol. Phys.* **2005**, *103*, 3185.
[31] D. A. Kofke, P. T. Cummings, *Fluid Phase Equilibria* **1998**, *150–151*, 41.
[32] G. C. Boulougouris, I. G. Economou, D. N. Theodorou, *Mol. Phys.* **1999**, *96*, 905.
[33] G. C. Boulougouris, *J. Chem. Eng. Data* **2010**, *55*, 4140.
[34] M. Heidari, K. Kremer, R. Cortes-Huerto, R. Potestio, *J. Chem. Theory Comput.* **2018**, *14*, 3409.
[35] G. C. Boulougouris, *J. Phys. Chem. B* **2012**, *116*, 997.
[36] C. Perego, F. Giberti, M. Parrinello, *Eur. Phys. J. Spec. Top.* **2016**, *225*, 1621.
[37] H. Zhou, L. R. White, R. D. Tilton, *Colloids Surf. Physicochem. Eng. Asp.* **2006**, *277*, 119.
[38] B. Giera, L. A. Zepeda-Ruiz, A. J. Pascall, T. H. Weisgraber, *Langmuir* **2017**, *33*, 652.